Organic Electronics 60 (2018) 57–63

Contents lists available at ScienceDirect

Organic Electronics

journal homepage: www.elsevier.com/locate/orgel

High performance organo-lead halide perovskite light-emitting diodes via surface passivation of phenethylamine

Min Zhang[a,1], Fang Yuan[b,1], Wu Zhao[a,**], Bo Jiao[b], Chenxin Ran[b], Wenwen Zhang[d], Zhaoxin Wu[b,c,*]

[a] School of Information Science and Technology, Northwest University, Xi'an, Shannxi, 710069, People's Republic of China
[b] Key Laboratory of Photonics Technology for Information, Key Laboratory for Physical Electronics and Devices of the Ministry of Education, School of Electronic and Information Engineering, Xi'an Jiaotong University, Xi'an, 710049, People's Republic of China
[c] Collaborative Innovation Center of Extreme Optics, Shanxi University, Taiyuan, 030006, China
[d] School of Electronic Engineering, Xi'an University of Post & Telecommunication, Xi'an, 710121, China

ARTICLE INFO

Keywords:
Lead halide perovskites
Perovskite light-emitting diodes
Surface passivation
Phenethylamine

ABSTRACT

One of the organometal halide perovskite materials, *i.e.* methylammonium lead bromide ($MAPbBr_3$), possesses interesting and incredible physicochemical properties, and shows great promising in light-emitting device. However, the poor morphology and high defect density properties of $MAPbBr_3$ films limit the performance of perovskite light-emitting diodes (PeLEDs). Here, high efficiency PeLEDs based on $MAPbBr_3$ is demonstrated by the incorporation of phenethylamine (PEA). We find that the introduction of PEA into the precursor of $MAPbBr_3$ reduces the grain size and increases the coverage of $MAPbBr_3$ films. In addition, it also passivates the surface defects of the grains, which all lead to high photoluminescence efficiency. In order to promote the charge injection into the $MAPbBr_3$ grains, suppress the exciton quenching at the interface of perovskite film and hole transporting layer (HTL)/electron transporting layer (ETL), the device structure of "insulator-perovskite-insulator" is employed to further improve the performance of the PeLEDs. Under optimized ratio of MA and PEA, a maximum current efficiency 9.81 cd A^{-1} is achieved. Our work presents an facile and robust route for high performance PeLEDs.

1. Introduction

Recently, organic–inorganic lead halide perovskite materials, with a three-dimensional ABX_3 structure (where A for methylamine ($CH_3NH_3^+$, MA) or formamidine ($HC(NH_2)_2^+$, FA) cation; B for Pb^{2+}, Sn^{2+} or Ge^{2+} metal ion; X for I^-, Br^-, Cl^- halide ion [1,2]), have attracted considerable interests in optoelectronic applications owing to their interesting and incredible physicochemical properties [3–5], such as facile solution process ability [6–9], balanced charge transport properties with long diffusion lengths [10,11], tunable band-gaps [12–14], high carrier mobilities [15–17], and low non-radiative recombination ascribed to their unique defect chemistry [18,19]. Moreover, the demonstration of high photoluminescence (PL) quantum efficiency in the hybrid perovskite suggests effective light emitters for light-emitting diodes, and the optical absorbance can be easily tuned across the entire visible spectrum *via* halogen substitutions [20–23].

Since the first realization of perovskite light-emitting diodes (PeLEDs) at room temperature pioneered by R. Friend and his coworkers in 2014 [24], organic–inorganic lead halide perovskite materials have been at the basis of several breakthroughs in the development of light-emitting devices. So far, H. Cho et al. overcame the electroluminescence efficiency limitation of PeLEDs and made a breakthrough in current efficiency (CE) of the device up to 42.9 cd A^{-1} and external quantum efficiency (EQE) to 8.53% within only one year [25]. However, the efficiency of PeLEDs is intrinsically limited by poor coverage and big grains of the perovskite film directly prepared by a one-step spin-coating method from its pure precursor solution, resulting in serious non-radiative leakage current losses in the PeLEDs. So far, a number of approaches have been developed to overcome those problems. In the preparation process of perovskite thin films, anti-solvents such as chlorobenzene, toluene, and diethyl ether are used to control the formation process of the perovskite film to achieve a uniform and

* Corresponding author. Key Laboratory of Photonics Technology for Information, Key Laboratory for Physical Electronics and Devices of the Ministry of Education, School of Electronic and Information Engineering, Xi'an Jiaotong University, Xi'an, 710049, People's Republic of China.
** Corresponding author.
E-mail addresses: zhaowu@nwu.edu.cn (W. Zhao), zhaoxinwu@mail.xjtu.edu.cn (Z. Wu).
[1] These two authors contributed equally to the work.

https://doi.org/10.1016/j.orgel.2018.05.026
Received 13 February 2018; Received in revised form 16 May 2018; Accepted 19 May 2018
Available online 21 May 2018
1566-1199/

smooth surface [26,27]. These interfacial treatments, however, are complex and delicate, which limits the reproducibility of the fabrication process of the perovskite film. In addition, two-step methods have been widely adopted to attain uniform perovskite films [28]. However, these methods could lead to reduced grain size and poor crystallinity of perovskite films, resulting in high defect density and thereby inferior luminescent properties. Therefore, preparation of smooth perovskite films with full coverage and passivation of the grain surface are still open problems to be solved for the high performance PeLEDs.

In this work, we introduce phenethylamine (PEA) into methylammonium lead bromide ($MAPbBr_3$) system to improve the performance of PeLEDs devices based on $MAPbBr_3$ thin film. PEA is found to effectively improve the coverage and passivate the surface defect of $MAPbBr_3$ film. By utilizing the device structure of "insulator-perovskite-insulator" that we developed recently, an efficient green emission with luminance of 29268 cd m^{-2} and the maximum current efficiency of 9.81 cd A^{-1} with promising device stability can be achieved.

2. Experimental section

2.1. Perovskite precursor

A 38 wt% $MAPbBr_3$ perovskite precursor solutions ($PbBr_2$:MABr molar ratio = 1:1.5) were prepared by dissolving $PbBr_2$ (Aldrich, 99.999%) and MABr (Borun New Material Technology LTD) in anhydrous dimethylformamide (DMF), and then stirred at 60 °C for 2 h in a nitrogen-filled glove box. After that, 1 μl, 3 μl, 5 μl, 10 μl and 20 μl PEA solutions (Acros Organics, 99%) were separately added into 1 ml of the above-mentioned $MAPbBr_3$ precursor solutions in which the final volume ratios of PEA solution to $MAPbBr_3$ precursor solution is 0.1%, 0.3%, 0.5%, 1% and 2%, respectively. After stirring at 60 °C for 1 h in a nitrogen-filled glove box, the hybrid precursor solutions were obtained.

2.2. Fabrication of PeLEDs

Firstly, indium tin oxide (ITO) patterned glass substrates with sheet resistance of about 15 Ω/square were cleaned with deionized water and organic solvents, and then exposed to UV–ozone ambience for 5 min. Secondly, the substrates were transported into a vacuum chamber, and then 3 nm LiF (Sigma-Aldrich, 99.999%) layer was deposited onto the ITO-coated substrates via thermal evaporation under high vacuum ($< 3 \times 10^{-3}$ Pa) with the rate of about 0.2 Å/s monitored in situ by a quartz-crystal sensor. After deposition, the ITO/LiF substrates were transferred into a nitrogen-filled glove box in which the above-mentioned perovskite precursors were spin-coated (3000 rpm for 30 s) onto the substrates and then annealed at 80 °C for 15 min to form the perovskite layer. Finally, these substrates were transported into the vacuum chamber again, and then, LiF (8 nm)/Bphen (60 nm)/LiF (1 nm)/Al (100 nm) were sequentially deposited onto the substrates under a pressure of 3×10^{-3} Pa at a rate of about 0.2 Å s^{-1}, 1 Å s^{-1}, 0.2 Å s^{-1} and 5 Å s^{-1}, respectively. In our experiments, the light emitting devices have an effective area of about 12 mm^2.

2.3. Sample characterization

Film thickness of the samples was measured with ellipsometry (SE MF-1000, Korea). The surface of perovskite layer was investigated by scanning electron microscopy (SEM, Quanta 250, FEI). The crystalline structure of the perovskite layer on ITO substrate was determined by X-ray diffraction (XRD, D/MAX-2400, Rigaku, Japan) with Cu-Kα radiation. The absorption and PL spectra were obtained by a UV–vis spectrophotometer (HITACHI U-3010, Japan) and a fluorescence spectrometer (Fluoromax-4 spectrofluometer), respectively. Time-resolved PL spectra were recorded with 50 ps time resolution using time-correlated single photon counting (TCSPC) system (FLS920 spectrometer) (excited by picosecond pulsed LEDs, pulse duration, < 850 ps, repetition rate, 10 MHz). The luminance-current-voltage (L-I-V) characteristics of the devices were measured using a computer-controlled source meter (Keithley 2602) and a calibrated silicon photodiode. The EL spectra were collected by a PR650 spectrometer. All light emitting measurements were carried out in a nitrogen-filled glove box at room temperature.

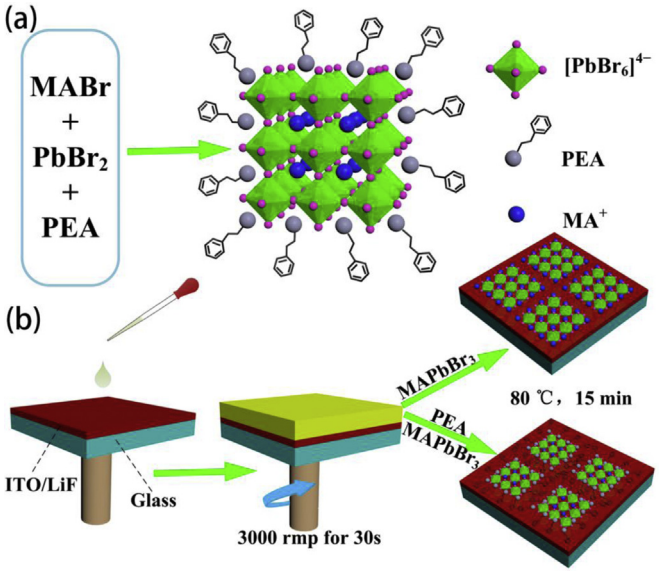

Fig. 1. (A) The design of $MAPbBr_3$ with chemically addressable ligands. The inorganic layers consist of corner-sharing lead bromide octahedra in which the black and pink balls represent Pb and Br atoms, respectively. The organic layers consist of MA^+ cations and ligand PEA of blue and gray, respectively. (b) Schematic diagram of the $MAPbBr_3$ film formation process. (For interpretation of the references to colour in this figure legend, the reader is referred to the Web version of this article.)

3. Results and discussion

By using one-step solution process, the schematic diagram of the $MAPbBr_3$ structural change after PEA introduction is shown in Fig. 1a. In the (PEA) (MA)$PbBr_3$ perovskite, small fraction of three-dimensional (3D) $MAPbBr_3$ cluster is protected by long-chain PEA ions, which greatly improves the stability of the $MAPbBr_3$ crystal structure. The discrete quantum level generated by this "quantum well" structure is reported to be more conducive to the selective carrier transport [5,29]. As shown in Fig. 1b, we fabricated the device by introducing different amounts of PEA into $MAPbBr_3$ precursor solution, and then spin-coating onto an indium tin oxide (ITO) substrate covered with a thin LiF layer followed by post-annealing (see Experimental Section).

The surface morphology and microstructure of the perovskite film have a critical impact on the performance parameters of the device. SEM images of $MAPbBr_3$ films fabricated with different amounts of PEA in $MAPbBr_3$ precursor solution is shown in Fig. 2a–f. As shown in Fig. 2a, when no PEA is introduced, the perovskite film with large grains and low surface coverage can be observed. When the PEA ratio increases to 0.1%, the surface coverage of $MAPbBr_3$ film begins to increase, though the grain size is not found to reduce, as shown in Fig. 2b. Furthermore, when the PEA ratio increases to 0.3%, the surface coverage of resultant film is significantly improved and the crystal size is relatively reduced as shown in Fig. 2c. While the PEA ratio exceeds 0.3%, the surface coverage of $MAPbBr_3$ film gradually increases as shown in Fig. 2d–f. As depicted, the surface coverage of the $MAPbBr_3$ film is significantly increased with increasing dosage of PEA, especially, the surface coverage reaches 100% when the dosage of PEA is more than 1%.

The crystallinity of the perovskite films is also verified by XRD. As

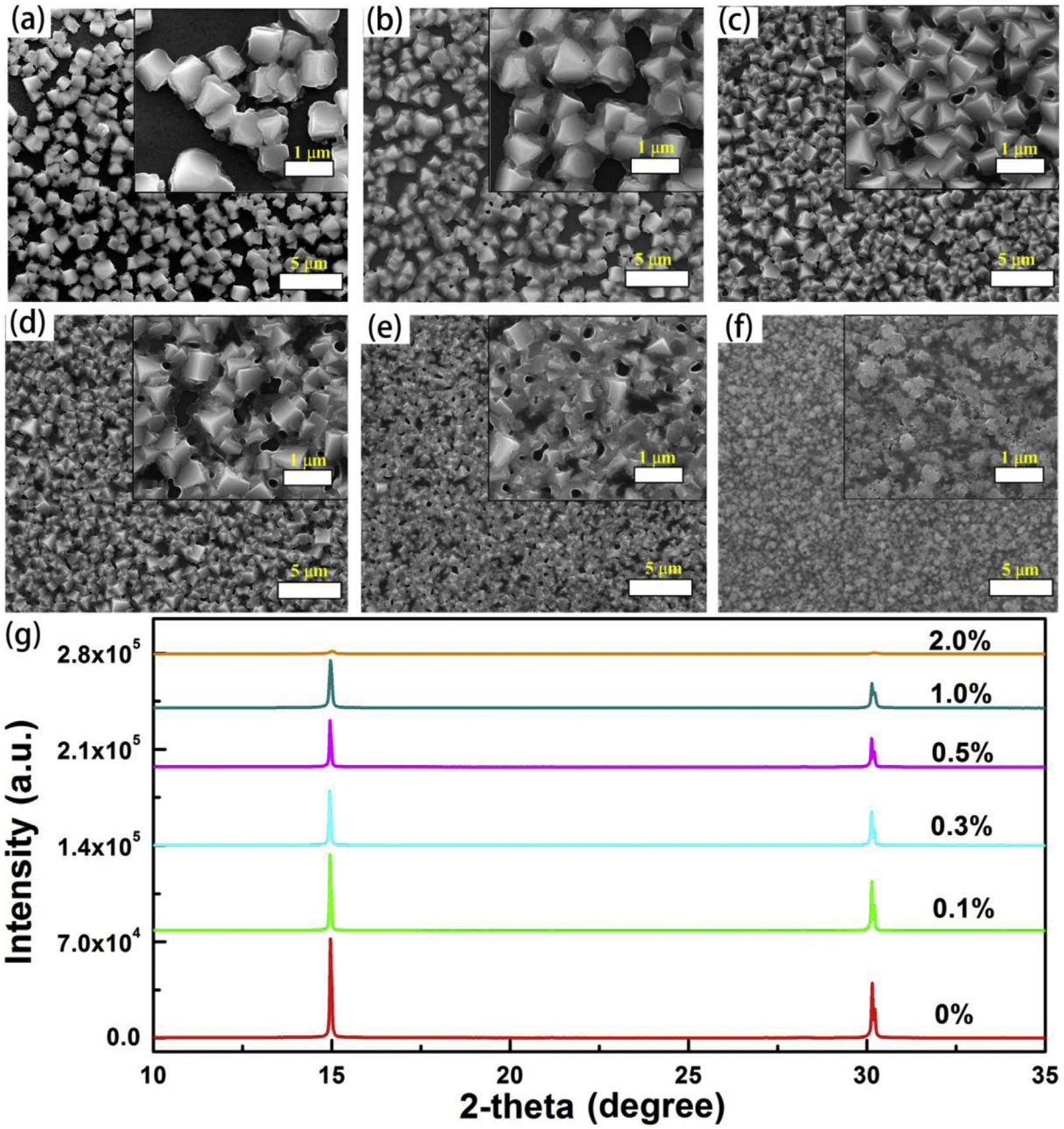

Fig. 2. Top-view SEM images of $MAPbBr_3$ films fabricated with different volume PEA of 0% (a), 0.1% (b), 0.3% (c), 0.5% (d), 1% (e) and 2% (f), respectively. (g) XRD patterns of perovskite films prepared by different ratios of PEA.

shown in Fig. 2g, the $MAPbBr_3$ films fabricated with different amounts of PEA show diffraction peaks at 14.9° and 30.03°, which can be assigned to (100) and (200) facets of a cubic perovskite structure, respectively [30,31]. Increasing of PEA dosage causes the decrement in peak intensity, and the peaks almost vanish for 2% of PEA dosage. This result demonstrates that the crystallinity of $MAPbBr_3$ perovskite crystal deteriorates, which can also be verified by SEM images. We speculated that the introduction of PEA into the perovskite precursor solution may suppress the crystal growth of $MAPbBr_3$ [32,33].

In order to further explore the role of PEA in the formation of the $MAPbBr_3$ crystal, optically pumped experiments were carried out to estimate the trap state density in the films. The $MAPbBr_3$ films with different amounts of PEA (0%, 0.3% and 1%) on glass substrates are excited at 400 nm by a frequency-doubled Ti:sapphire femtosecond laser oscillator delivering 150 fs pulses at a 1 kHz repetition rate. Through a pinhole filter and a positive lens, the laser beam forms a 3 mm diameter spot and is irradiated obliquely onto the surface of the samples. Face emission spectra were collected directly into a fiber optic spectrometer. The measured output emission spectra and the input-output intensity of the samples as a function of increasing pump energy are shown in Fig. 3a–c. The first intersection represents the pump energy needed to fill all the traps (*i.e.*, the threshold trap pump energy P_{trap}). As shown in Fig. 3, P_{trap} of the $MAPbBr_3$ films with different amounts of PEA 0% (a), 0.3% (b) and 1% (c) are ~ 27, 14, and 11 $\mu J\,cm^{-2}$, respectively, corresponding to the calculated trap state densities of $\sim 6.37 \times 10^{17}$, 3.5×10^{17}, and $2.65 \times 10^{17}\,cm^{-3}$, respectively. In addition, to further explore the trap state densities of PEA (0.3%) in the formation of the $MAPbBr_3$ films, the bulk defects and surface traps were estimated with a formula as follows [34]:

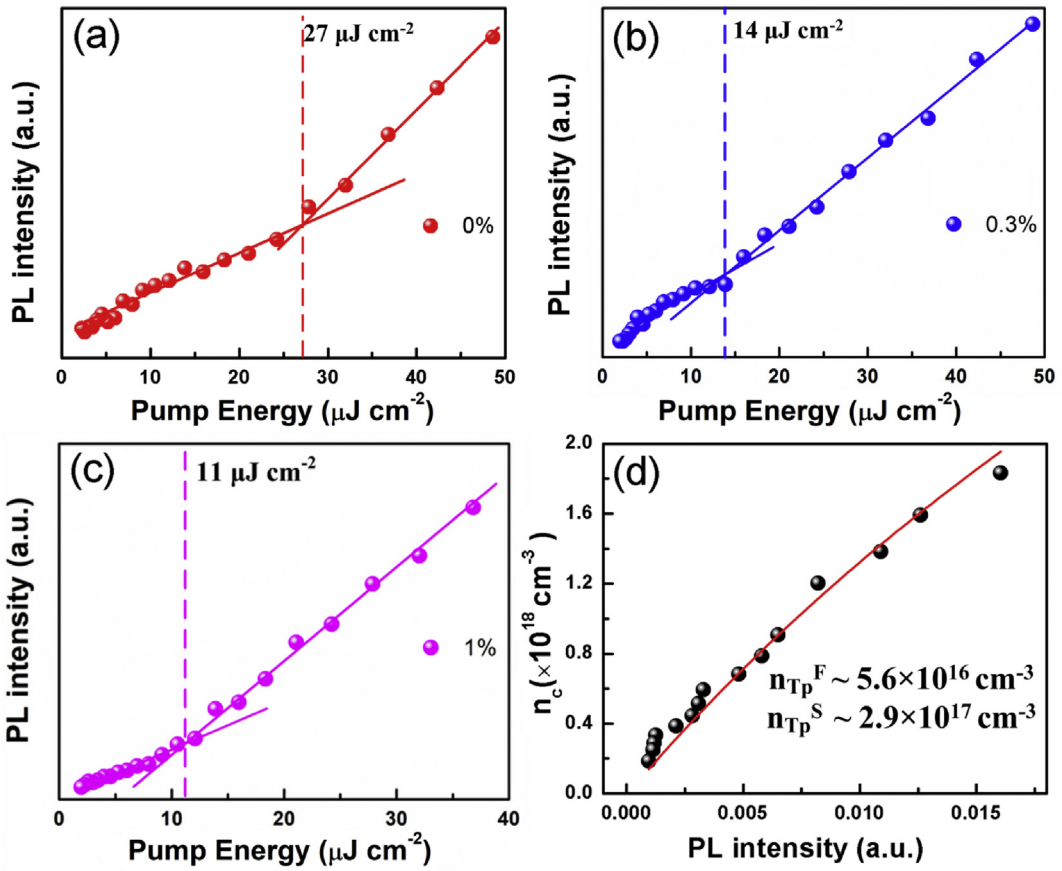

Fig. 3. The integrated emission intensity of the face emission spectra as a function of pump energy in the $MAPbBr_3$ films with different ratios of PEA 0% (a), 0.3% (b) and 1% (c) on glass substrates. (d) The experimental data with 0.3% PEA can be fitted using equation (1) for two types of trapping states.

$$n_c(0) = \sum_i n_{TP}^i(0)\left(1 - e^{-a_i t_0 I_{pL}/k}\right) + I_{pL}/k \quad (1)$$

Where n_{TP}^i is the trap states density, a_i is the product of the trapping cross section and the carrier velocity, k is a constant. The fitted values of bulk trap density and surface trap density is about 5.6×10^{16} and $2.9 \times 10^{17}\,cm^{-3}$, respectively, as shown in Fig. 3d. Obviously, the introduction of appropriate ratio of PEA (0.3%) could effectively improve the film quality, reduce the trap state density and lower the bulk trap density in the $MAPbBr_3$ films, and greatly improve the corresponding device performance. Although the introduction of excessive PEA further leads to lower trap density, in turn, the introduction of excess ligands molecules impairs the charge carrier transport and injection to the perovskite active layer, and has negative effects on the device, leading to a poor device performance.

The relationship between the emission properties and the perovskite film structures is studied using steady-state PL spectra, as shown in Fig. 4a., It is observed that the PL peaks have similar positions in all perovskite films with different amounts of PEA. The PL peaks of all perovskite films shift from $\lambda \approx 533$ nm to $\lambda \approx 528$ nm with increasing amounts of PEA. The blue-shift of PL spectra is attributed to the amine group of PEA, which results from the change of crystalline structure, film morphology, and the surface trap passivation effect [35]. As shown in Fig. 4a, the PL intensity elevated as the dosage of PEA increased. This increase in PL intensity can clearly be attributed to the surface coverage improvement of $MAPbBr_3$ films. As PEA is an insulating molecule, it will make short circuiting blockage in different layers across the active layer and confine the injected electrons and holes into the active layer for the radiative recombination, which causes the increase in PL intensity. However, excess introduction of PEA molecules, which impairs the charge carrier transport and injection to the perovskite active layer, negatively affects the performance of devices.

To further understand the photoelectric properties of these films, PL lifetime is estimated additionally, as shown in Fig. 4b. PL lifetime of the $MAPbBr_3$ is considered as the summation of quick and moderate decay components. The quick decay is identified with trap-associated recombination at grain limits, which is commonly known as a non-radiative process, though the slow or moderate decay is identified with radiative recombination inside the grains. Typically, the shorter lifetime indicates the higher recombination rate [23]. As can be seen in Fig. 4b, the PL lifetime is gradually extended with the increased amounts of PEA. This result indicates that the treatment of $MAPbBr_3$ by amine group in PEA can significantly reduce non-radiative recombination rate by decreasing the defect density.

In order to achieve the high performance of the PeLED device, the structure of "insulator-perovskite-insulator (IPI)" were employed, where a pair of ultrathin LiF films were used as insulating layers shown in Fig. 5a. IPI-structured PeLEDs had been reported in our previous work [36]. A series of PeLEDs with different thickness of LiF insulator layers were prepared so as to get the ideal device structure in this work as shown in Fig. S1. The optimized thicknesses of LiF at the two interfaces are 3 nm and 8 nm, respectively, as show in Fig. 5b. The ultrathin LiF films play two roles in devices, one is to induce carriers into perovskite crystals, improve their recombination and block the leakage current through the gaps or holes in perovskite films; the other is to avoid the exciton quenching at the interface between perovskite film and holes/electrons transport layer. From our previous report, the IPI-structured PeLEDs show the higher performance than that of conventional PeLEDs [36].

The luminance versus voltage (L–V) and current efficiency versus voltage characteristics of the devices are shown in Fig. 6a and b,

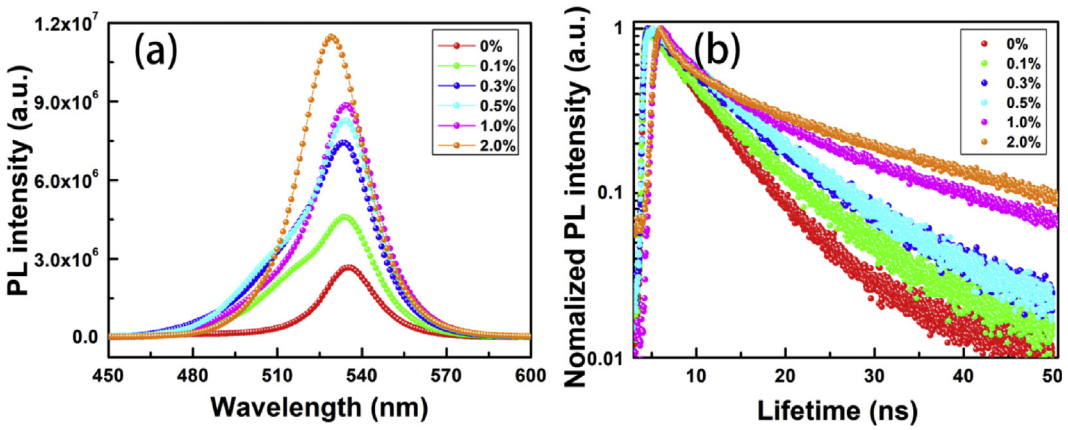

Fig. 4. (A) PL spectra and (b) PL lifetime curves of $MAPbBr_3$ thin films with different volumes PEA of 0%, 0.1%, 0.3%, 1% and 2%, respectively.

respectively, and the electroluminescent parameters are presented in Table 1. The turn-on voltage (while the luminance achieves 1 cd m^{-2}) of the films is around 3 V. This result shows the potential application in low driving voltage light-emitting devices. With a special structure and excellent $MAPbBr_3$ film, the most noteworthy luminance of 29268 cd m^{-2} is achieved at a driving voltage of just 10.2 V, and the maximum current efficiency of 9.81 cd A^{-1} at 8.2 V in the 0.3% PEA devices. It is worth to note that EL peaks of the devices shifted from $\lambda \approx 533$ nm to $\lambda \approx 528$ nm with increasing the doping content as shown in Fig. 6d, which is in agreement with the PL spectra in all the cases.

To correlate the relationship between the morphology of the $MAPbBr_3$ films and the performance of PeLEDs device, we further analyze the performance of the devices. The current efficiency of 3.3 cd A^{-1} is achieved in the 0% PEA devices. The low current efficiency is due to the large particles and great amount of pinholes, which also led to contact between ITO and Bphen, though a IPI structure is used. While after the introduction of 0.1% PEA in $MAPbBr_3$, the number of pinholes reduces and the surface coverage improves, as evidenced in Fig. 2a. Because the $MAPbBr_3$ film shows low coverage, the device still has a low current efficiency and luminance. Despite of this, the current injection still becomes easier compared to 0% PEA devices. When PEA increased to 0.3%, a maximum luminance of 29268 cd m^{-2} and a current efficiency of 9.81 cd A^{-1} can be obtained. The morphology of the $MAPbBr_3$ film is significantly improved and the crystal size is relatively reduced, which makes current injection much easier. In addition, the amine group of PEA can passivate the surface of $MAPbBr_3$ as evidenced in Fig. 3, which leads to lower defect concentration and the best performance of PeLEDs. When PEA exceed 0.3%, the morphology of $MAPbBr_3$ film become more and more uniform and smooth, but the PeLEDs performance is getting worse. As shown in Fig. 6c, further increasing the PEA dosage results in the decreased carrier transport of the PeLEDs, thus the performance of PeLED is deteriorated. To further study the effect of PEA on the stability of the PeLEDs, we have measured the performance of the device with multiple scans from the same PeLED as shown in Fig. S2, the stability of the PeLEDs increases as the PEA content gradually increasing under same test conditions. Therefore, the addition of PEA is evidently beneficial to the stability of PeLEDs.

4. Conclusion

In summary, we have presented a facile one-step method to produce high current efficiency PeLEDs by introducing the PEA into $MAPbBr_3$ system. It is found that the introduction of PEA favors the formation of smaller grains, increases the coverage of $MAPbBr_3$ films, and also passivates the surface of $MAPbBr_3$ grains. Based on advanced IPI device structure, we obtained an efficient green emission PeLED with the most noteworthy luminance of 29268 cd m^{-2} and the maximum current efficiency of 9.81 cd A^{-1} in the 0.3% PEA devices. In addition, the introduction of PEA can also improve the stability of PeLEDs. Our work demonstrate a facile and robust method to increase coverage and reduce defect states of thin $MAPbBr_3$ films, which will be of great significance for improving the performance of PeLEDs.

Acknowledgment

This work was financially supported by National Natural Science Foundation of China (Grant No. 11574248), National Key R&D Program of China (Grant No. 2016YFB0400702), International Cooperation by Shaanxi (Grant No. 2015KW-008), China Postdoctoral Science Foundation (Grant No. 2016M590947), National Natural Science Foundation of China (Grant No. 61505161), Natural Science Basic Research Plan of Shaanxi Province (Grant No. 2017JM6064), Scientific Research Plan Projects of Shaanxi Education Department (Grant No. 17JK0700) and the Fundamental Research Funds for the Central Universities (Grant No. xjj2016031). The SEM work was implemented at International Centre for Dielectric Research (ICDR), Xi'an Jiaotong

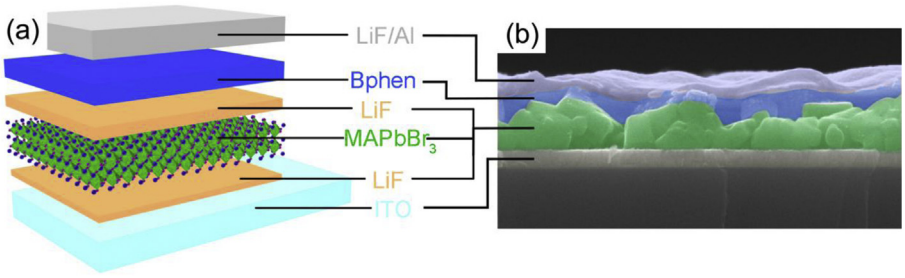

Fig. 5. (A) Schematic illustration of the $MAPbBr_3$-based PeLEDs structure: ITO/LiF (3 nm)/$MAPbBr_3$/LiF (8 nm)/Bphen (60 nm)/LiF (1 nm)/Al (100 nm). (b) Cross section SEM image of the PeLED with 0% PEA.

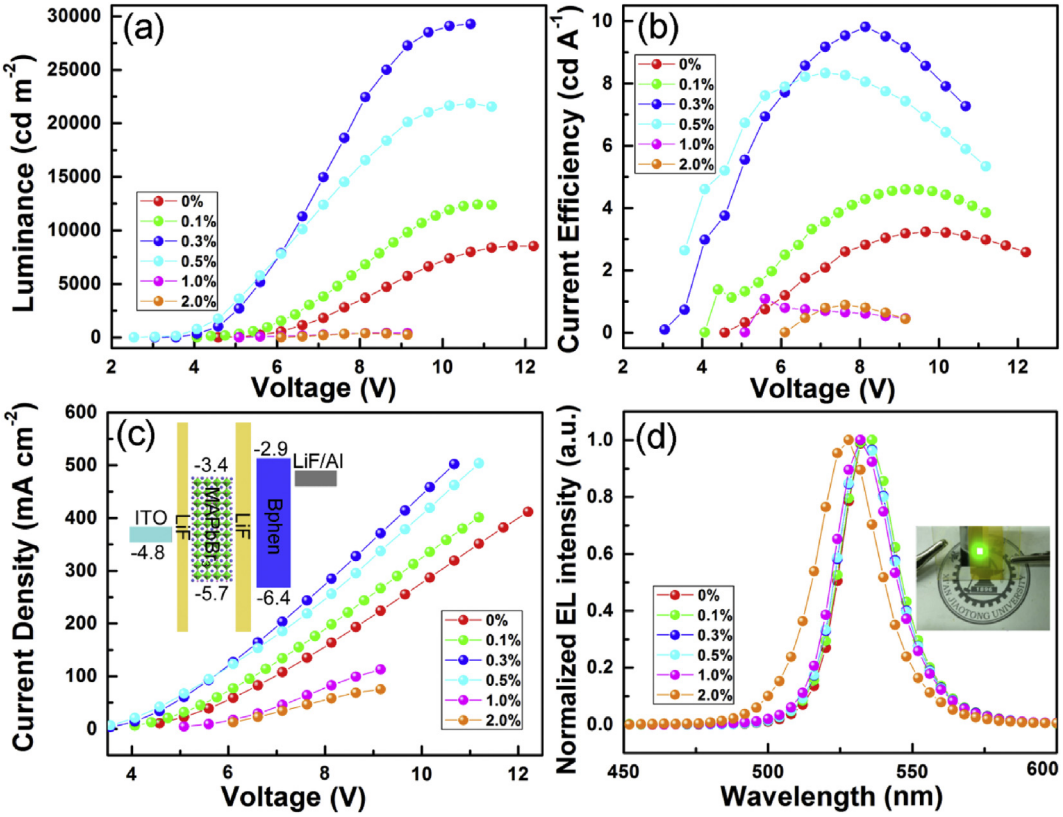

Fig. 6. (A) Luminance versus voltage characteristics, (b) current efficiency versus voltage characteristics, (c) Current density versus voltage characteristics, Inset of (c): the energy level diagram of the PeLED. (d) Electroluminescence spectrum of PeLEDs with different volume ratios of PEA, Inset of (d): the photograph of functional PeLED with 0.3% PEA.

Table 1
The properties of PeLEDs with different volume ratios of PEA.

PEA Volume ratio	EL Peak (nm)	PL Peak (nm)	CE (cd A^{-1})	Luminance (cd m^{-2})
0%	533	533	3.3	8558
0.1%	533	533	4.6	12420
0.3%	533	533	9.81	29268
0.5%	533	533	8.33	21865
1.0%	533	533	1.08	423
2.0%	528	528	0.88	375

University, Xi'an, China. The authors also thank Mr. Ma for his help in using SEM.

Appendix A. Supplementary data

Supplementary data related to this article can be found at http://dx.doi.org/10.1016/j.orgel.2018.05.026.

References

[1] A. Kojima, K. Teshima, Y. Shirai, T. Miyasaka, Organometal halide perovskites as visible-light sensitizers for photovoltaic cells, J. Am. Chem. Soc. 131 (2009) 6050–6051.
[2] H.S. Kim, H.I. Sang, N.G. Park, Organolead halide perovskite: New horizons in solar cell research, J. Phys. Chem. C 118 (2014) 5615–5625.
[3] J. Xi, Z. Wu, B. Jiao, H. Dong, C. Ran, C. Piao, T. Lei, T.B. Song, W. Ke, T. Yokoyama, Multichannel interdiffusion driven $FASnI_3$ film formation using aqueous hybrid salt/polymer solutions toward flexible lead-free perovskite solar cells, Adv. Mater. 29 (2017) 1606964.
[4] F. Yuan, Z. Wu, H. Dong, J. Xi, K. Xi, G. Divitini, B. Jiao, X. Hou, S. Wang, Q. Gong, High stability and ultralow threshold amplified spontaneous emission from formamidinium lead halide perovskite films, J. Phys. Chem. C 121 (2017) 15318–15325.
[5] N. Wang, L. Cheng, R. Ge, S. Zhang, Y. Miao, W. Zou, C. Yi, Y. Sun, Y. Cao, R. Yang, Perovskite light-emitting diodes based on solution-processed self-organized multiple quantum wells, Nat. Photon. 10 (2016) 699.
[6] J. Burschka, N. Pellet, S.J. Moon, R. Humphrybaker, P. Gao, M.K. Nazeeruddin, M. Grätzel, Sequential deposition as a route to high-performance perovskite-sensitized solar cells, Nature 499 (2013) 316–319.
[7] Q. Chen, H. Zhou, Z. Hong, S. Luo, H.-S. Duan, H.-H. Wang, Y. Liu, G. Li, Y. Yang, Planar heterojunction perovskite solar cells via vapor-assisted solution process, J. Am. Chem. Soc. 136 (2013) 622–625.
[8] G.E. Eperon, V.M. Burlakov, P. Docampo, A. Goriely, H.J. Snaith, Morphological control for high performance, solution-processed planar heterojunction perovskite solar cells, Adv. Funct. Mater. 24 (2014) 151–157.
[9] J. You, Z. Hong, Y.M. Yang, Q. Chen, M. Cai, T.-B. Song, C.-C. Chen, S. Lu, Y. Liu, H. Zhou, Low-temperature solution-processed perovskite solar cells with high efficiency and flexibility, ACS Nano 8 (2014) 1674–1680.
[10] S. Bai, Z. Wu, X. Wu, Y. Jin, N. Zhao, Z. Chen, Q. Mei, X. Wang, Z. Ye, T. Song, High-performance planar heterojunction perovskite solar cells: preserving long charge Carrier diffusion lengths and interfacial engineering, Nano Res. 7 (2014) 1749–1758.
[11] H. Yan, B. An, Z. Fan, X. Zhu, X. Lin, Z. Jin, G. Ma, Ultrafast terahertz probe of photoexcited free charge carriers in organometal $CH_3NH_3PbI_3$ perovskite thin film, Appl. Phys. a 122 (2016) 414.
[12] V. D'Innocenzo, A.R. Srimath Kandada, M. De Bastiani, M. Gandini, A. Petrozza, Tuning the light emission properties by band gap engineering in hybrid lead halide perovskite, J. Am. Chem. Soc. 136 (2014) 17730–17733.
[13] S.A. Kulkarni, T. Baikie, P.P. Boix, N. Yantara, N. Mathews, S. Mhaisalkar, Band-gap tuning of lead halide perovskites using a sequential deposition process, J. Mater. Chem. 2 (2014) 9221–9225.
[14] Z. Chen, C. Zhang, X.F. Jiang, M. Liu, R. Xia, T. Shi, D. Chen, Q. Xue, Y.J. Zhao, S. Su, High-performance color-tunable perovskite light emitting devices through structural modulation from bulk to layered film, Adv. Mater. 29 (2017) 1603157.
[15] H. Zhou, Q. Chen, G. Li, S. Luo, T.B. Song, H.S. Duan, Z. Hong, J. You, Y. Liu, Y. Yang, Photovoltaics. Interface engineering of highly efficient perovskite solar cells, Science 345 (2014) 542–546.
[16] H. Dong, Z. Wu, J. Xi, X. Xu, L. Zuo, T. Lei, X. Zhao, L. Zhang, X. Hou, A.K.Y. Jen, Pseudohalide-induced recrystallization engineering for $CH_3NH_3PbI_3$ film and its application in highly efficient inverted planar heterojunction perovskite solar cells, Adv. Funct. Mater. 28 (2018) 1704836.
[17] F. Yuan, J. Xi, H. Dong, K. Xi, W. Zhang, C. Ran, B. Jiao, X. Hou, K.Y. Jen, Z. Wu, All-inorganic hetero-structured cesium tin halide perovskite light-emitting diodes with current density over 900 A cm^{-2} and its amplified spontaneous emission behaviors, Phys. Status Solidi RRL 12 (2018) 1800090.

[18] Y. Shao, Z. Xiao, C. Bi, Y. Yuan, J. Huang, Origin and elimination of photocurrent hysteresis by fullerene passivation in $CH_3NH_3PbI_3$ planar heterojunction solar cells, Nat. Commun. 5 (2014) 5784.
[19] Y. Shi, J. Xi, T. Lei, F. Yuan, J. Dai, C. Ran, H. Dong, B. Jiao, X. Hou, Z. Wu, Rubidium doping for enhanced performance of highly efficient formamidinium-based perovskite light-emitting diodes, ACS Appl. Mater. Interfaces 10 (2018) 9849–9857.
[20] Z. Wang, T. Cheng, F. Wang, S. Dai, Z. Tan, Morphology engineering for high-performance and multicolored perovskite light-emitting diodes with simple device structures, Small 12 (2016) 4412–4420.
[21] Y.H. Kim, H. Cho, J.H. Heo, T.S. Kim, N.S. Myoung, C.L. Lee, S.H. Im, T.W. Lee, Multicolored organic/inorganic hybrid perovskite light-emitting diodes, Adv. Mater. 27 (2015) 1248–1254.
[22] N.K. Kumawat, A. Dey, A. Kumar, S.P. Gopinathan, K.L. Narasimhan, D. Kabra, Band gap tuning of $CH_3NH_3Pb(Br_{1-x}cl_x)_3$ hybrid perovskite for blue electroluminescence, ACS Appl. Mater. Interfaces 7 (2015) 13119–13124.
[23] F. Zhang, H. Zhong, C. Chen, X.G. Wu, X. Hu, H. Huang, J. Han, B. Zou, Y. Dong, Brightly luminescent and color-tunable colloidal CH_3NH_3PbX3 (X = Br, I, Cl) quantum dots: potential alternatives for display technology, ACS Nano 9 (2015) 4533–4542.
[24] Z.K. Tan, R.S. Moghaddam, M.L. Lai, P. Docampo, R. Higler, F. Deschler, M. Price, A. Sadhanala, L.M. Pazos, D. Credgington, Bright light-emitting diodes based on organometal halide perovskite, Nat. Nanotechnol. 9 (2014) 687–692.
[25] H. Cho, S.H. Jeong, M.H. Park, Y.H. Kim, C. Wolf, C.L. Lee, J.H. Heo, A. Sadhanala, N. Myoung, S. Yoo, Overcoming the electroluminescence efficiency limitations of perovskite light-emitting diodes, Science 350 (2015) 1222–1225.
[26] J.C. Yu, D.W. Kim, D.B. Kim, E.D. Jung, K.S. Lee, S. Lee, D.D. Nuzzo, J.S. Kim, M.H. Song, Effect of the solvent used for fabrication of perovskite films by solvent dropping on performance of perovskite light-emitting diodes, Nanoscale 9 (2017) 2088–2094.
[27] Y.K. Chih, J.C. Wang, R.T. Yang, C.C. Liu, Y.C. Chang, Y.S. Fu, W.C. Lai, P. Chen, T.C. Wen, Y.C. Huang, NiOx electrode interlayer and $CH_3NH_2/CH_3NH_3PbBr_3$ interface treatment to markedly advance hybrid perovskite-based light-emitting diodes, Adv. Mater. 28 (2016) 8687–8694.
[28] Y. Chen, M. He, J. Peng, Y. Sun, Z. Liang, Structure and growth control of organic–inorganic halide perovskites for optoelectronics: from polycrystalline films to single crystals, Adv. Sci. 3 (2016) 1500392.
[29] X. Zhang, H. Lin, H. Huang, C. Reckmeier, Y. Zhang, W.C.H. Choy, A.L. Rogach, Enhancing the brightness of cesium lead halide perovskite nanocrystal based green light-emitting devices through the interface engineering with perfluorinated ionomer, Nano Lett. 16 (2016) 1415–1420.
[30] H.S. Kim, C.R. Lee, J.H. Im, K.B. Lee, T. Moehl, A. Marchioro, S.J. Moon, R. Humphry-Baker, J.H. Yum, J.E. Moser, Lead iodide perovskite sensitized all-solid-state submicron thin film mesoscopic solar cell with efficiency exceeding 9%, Sci. Rep. 2 (2012) 591.
[31] N.K. Kumawat, A. Dey, K.L. Narasimhan, D. Kabra, Near infrared to visible electroluminescent diodes based on organometallic halide perovskites: structural and optical investigation, ACS Photonics 2 (2015) 349–354.
[32] J. Byun, H. Cho, C. Wolf, M. Jang, A. Sadhanala, R.H. Friend, H. Yang, T.W. Lee, Efficient visible Quasi-2D perovskite light-emitting diodes, Adv. Mater. 28 (2016) 7515–7520.
[33] C. Ran, J. Xi, W. Gao, F. Yuan, T. Lei, B. Jiao, X. Hou, Z. Wu, Bilateral interface engineering toward efficient 2D-3D bulk heterojunction tin halide lead-free perovskite solar cells, ACS Energy Lett. 3 (2018) 713–721.
[34] G. Xing, N. Mathews, S.S. Lim, N. Yantara, X. Liu, D. Sabba, M. Grätzel, S. Mhaisalkar, T.C. Sum, Low-temperature solution-processed wavelength-tunable perovskites for lasing, Nat. Mater. 13 (2014) 476–480.
[35] M. Wei, W. Sun, Y. Liu, Z. Liu, L. Xiao, Z. Bian, Z. Chen, Highly luminescent and stable layered perovskite as the emitter for light emitting diodes, Phys. Status Solidi 213 (2016) 2727–2732.
[36] Y. Shi, W. Wu, H. Dong, G. Li, K. Xi, G. Divitini, C. Ran, F. Yuan, M. Zhang, B. Jiao, X. Hou, Z. Wu, A strategy for architecture design of crystalline perovskite light-emitting diodes with high performance, Adv. Mater. (2018) 1800251https://doi.org/10.1002/adma.201800251.